Analyses of Particle and Energy Balances using a Core-SOL-Divertor (CSD) Model for Tokamak DEMO-Reactor Studies

Kazuhiro YAMADA[1,2], Kazuo HOSHINO[2] and Akiyoshi HATAYAMA[2]

[1]*Central Japan Railway Company, Komaki 485-0801, Japan*
[2]*Keio University, Yokohama 223-8522, Japan*

(Received 21 February 2024 / Accepted 9 October 2024)

Understanding of key physics and engineering parameters is one of the most important issues to conduct fundamental design studies of future fusion reactors. Also, sensitivity analyses of performance by parameter surveys need to be done for optimizing a reactor. This research aims at a qualitative analysis to identify directions of design parameter optimization for fusion reactors. For this purpose, a Core-SOL-Divertor (CSD) model has been employed, because it is suitable for a wide range of parameter surveys by changing various parameters with low computational costs. This paper analyzes the particle and energy balances of the JT-60U divertor plasma by using a CSD model and reveals dependencies of the balances on design parameters of the device. In addition, the same CSD model is applied to conduct divertor plasma analyses for a future demonstration reactor (JA-DEMO). The result shows that it is possible to obtain a low temperature state of its divertor plasma as has been already reported by a two-dimensional SOL-Divertor integrated code. From these results, this paper shows that the CSD model is applicable to basic studies of directions and design concepts for future fusion reactors.

Keywords: CSD model, parameter survey, sensitivity analysis, JT-60U, JA DEMO

DOI: 10.1585/pfr.19.1403034

1. Introduction

One of the most critical issues to design future demonstration and/or commercial fusion reactors is how to control high heat load on divertor plates. Two-dimensional (2D) integrated codes such as SONIC [1, 2] or SOLPS-ITER [3,4] are widely used for understanding of behaviors of boundary plasmas [5–8]. However, calculation costs with these heavy codes are high. Low costs and simple models are suitable to understand basic behaviors of fusion plasmas and to conduct fundamental and conceptual design studies of future fusion reactors over a wide range of physics and engineering parameters.

Core-SOL-Divertor (CSD) models [9–11] were proposed as one of the useful simple models describing SOL and divertor plasmas. CSD models are based on so-called zero-dimensional (0D) models for the core, SOL and divertor regions. Zero-dimensional models treat each region as a point by using local or averaged quantities of basic plasma parameters, such as plasma density, flow velocity and temperature. A distinctive feature of CSD models different from other two-point models for the SOL and divertor plasmas [12, 13] is that CSD models include the core plasma as well as the SOL and divertor plasmas. Although the core plasma is also modelled by a very simple 0D model of particle and energy balance equations in CSD models, they are possible to perform integrated and self-consistent analyses of basic characteristics and/or performances for the fusion core, SOL and divertor plasmas altogether.

Reference [11] has shown the particle/energy balances on (T_d, n_d) plane. It has also discussed state transitions between high/low recycling while changing relations among three decay length (density/temperature/energy) equivalent to SOL width. This paper follows Ref. [11]. The particle/energy balances are thoroughly analyzed by using the CSD model with JT-60U parameters. This paper also evaluates dependencies of particle/energy balances on key physics and engineering parameters of the device.

Following the JT-60U divertor plasma analyses above, this research applies the CSD model to a simulation with JA DEMO parameters. For this simulation, both carbon and argon are calculated as impurity species. The CSD model compares impacts on the divertor plasma depending on the impurity species. A reproduction of a low temperature state of its divertor, which is shown by a SONIC simulation, proves that the CSD model has potential to perform basic studies of directions and design concepts for fusion reactors.

In Sec. 2, we first explain the CSD model. This paper mainly focuses on model equations for SOL and divertor plasmas. In Sec. 3, in order to solve simultaneous model equations, they are reduced to two main equations, i.e., particle/energy balance equations in SOL and divertor regions. After giving a summary-table comparing basic parameters for two tokamaks, a typical large tokamak ever existed (JT-60U) is calculated in Sec. 4.1 for the first case.

author's e-mail: kazuhiro.yamada@jr-central.co.jp

Then, in Sec. 4.2, particle/energy balance equations are analyzed to clarify dependencies of the divertor temperature on key physics and engineering parameters. In Sec. 5, a test calculation has been done by using input parameters relevant to a future demonstration fusion reactor (JA DEMO) to show potential of the CSD model for design studies of future fusion reactors.

2. Core-SOL-Divertor Model

2.1 Two-dimensional slab model

Figure 1 shows a schematic concept of the CSD model. By using toroidal symmetry, the geometry of single-null divertor tokamak in Fig. 1 (a) is simplified as a two-dimensional (2D) slab model geometry shown in Fig. 1 (b). The model geometry consists of three regions: i) core, ii) SOL and iii) divertor. In Fig. 1 (b), the x- and s-coordinates in the SOL and divertor regions correspond to the radial direction (perpendicular to the magnetic flux surface) and the direction along the magnetic field line, respectively. The length of the SOL and the divertor is expressed by L_s and L_d. Symbols Δ_n, Δ_T and Δ_E are the decay length for density, temperature and energy, respectively. In this paper, $\Delta_n = (1/2)\Delta_T$ and $\Delta_E = (2/7)\Delta_T$ are assumed.

As for the core region, we simply model it as a particles/energy source in the present study. In other words, as shown in Fig. 1 (b) we simply give the number of particles $\Phi_{sep}(s^{-1})$ and the heat Q_{sep} (W) across the separatrix boundary between the core and the SOL as input parameters.

2.2 Basic equations

The CSD model in this paper analyzes the left-half part of the slab model in Fig. 1 (b), which is terminated at the inner divertor target. This subsection provides basic equations of the CSD model.

(Particle Balance)

A particle transport equation was integrated over the SOL and the divertor regions with an assumption of exponential distribution of the density in the radial direction (the x-coordinate in Fig. 1 (b)). The decay length of exponential distribution is defined as Δ_n. Then, a particle balance equation is given as follows.

$$n_d M_d C_s 2\pi R_p \Delta_n \sin\psi - C_{in}^N \Phi_{sep} = f_{ion}\left(C_n n_d M_d C_s 2\pi R_p \Delta_n \sin\psi + N_{puff}\right). \quad (1)$$

For LHS (Left Hand Side), the first term shows the particle flux absorbed into the divertor target. The second term is the number of ion particles flowing into the left SOL from the core. The RHS (Right Hand Side) represents the ionization source due to neutral particles recycled and puffed at the target.

The gas puff is expressed by the term of N_{puff}. In the present study, $N_{puff} = 0$ is assumed. The symbol C_{in}^N is the fraction of the particles flowing into the left SOL in Fig. 1 (b) to all the particles from the core. This study assumes $C_{in}^N = 0.5$. Symbols n and T are the density and the temperature, respectively. The subscript "s" is for the SOL and "d" means the divertor. The symbol C_n is the ratio of the neutral flux from the divertor target to the plasma flux into the target. In this paper, $C_n = 1.0$ is assumed. Mach number at the divertor target is defined as $M_d = 1.0$. The symbol $C_s = \sqrt{T_d/m_i}$ is the sound velocity at the divertor target, where m_i is the proton mass. The major radius is expressed by R_p. The symbol ψ is the angle between the magnetic field and the divertor plate. In this study, $\sin\psi = 0.05$ is assumed. The symbol f_{ion} is the ionization faction of neutrals emitted from the divertor target. The faction f_{ion} is modelled in Sec. 2.3.

(Pressure Balance)

Integrating a momentum transport equation over the SOL and the divertor regions gives

$$(1 - f_{mom})\, n_s T_s = \left(1 + M_d^2\right) n_d T_d. \quad (2)$$

LHS of Eq. (2) expresses that the fraction, $(1 - f_{mom})$, of the

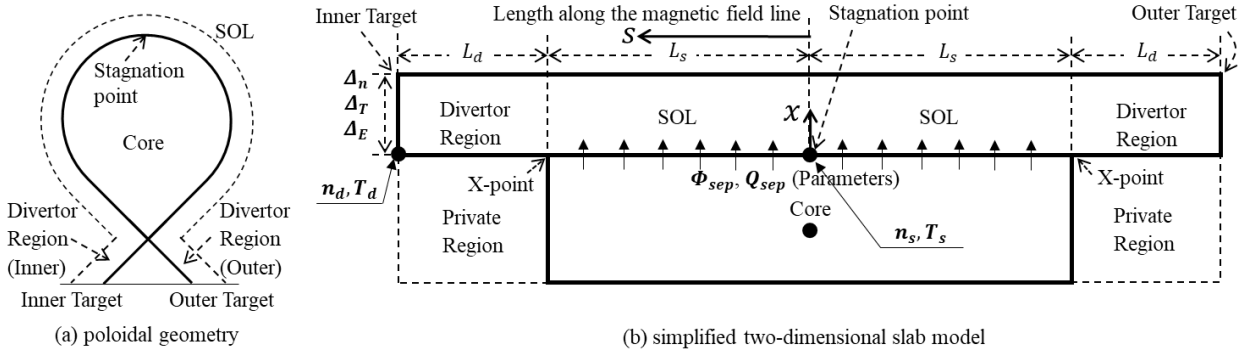

Fig. 1 Schematic drawing of the CSD model; (a) a poloidal cross section of single-null divertor tokamak and (b) a corresponding simplified two-dimensional slab model. In (b), the radial direction and the direction along the magnetic field line are taken as two basic directions of the (x, s) coordinate system by assuming toroidal symmetry in (a). The model consists of three regions: i) core, ii) SOL and iii) divertor with three representative points (solid circles) for each of them.

total pressure at the stagnation reaches the divertor target. The fraction f_{mom} is the ratio of momentum losses in both the SOL and the divertor regions to the static pressure at the stagnation point. The faction f_{mom} is modelled in Sec. 2.3. RHS means the total pressure just before the target.

(Global Energy Balance)

An energy transport equation was integrated over the SOL and the divertor regions with an assumption of exponential distribution of the heat flux in the radial direction. The decay length of exponential distribution is defined as Δ_E. Then, an energy balance equation is given as follows.

$$L_s q_\perp = f_{imp} L_s q_\perp + \varepsilon n_d M_d C_s \Delta_E + \gamma T_d n_d M_d C_s \Delta_E. \quad (3)$$

LHS of Eq. (3) is the heat crossing over the separatrix into the left-half part of the SOL in Fig. 1 (b). The first, second and third terms of RHS in Eq. (3) are impurity radiation losses, ionization losses and heat flux into the sheath region, respectively.

The SOL length is estimated as $L_s = \pi R_p q_{eff}$, where q_{eff} is the effective safety factor. The heat flux flowing into the left-half part of the SOL from the Core in Fig. 1 (b) is assumed to be $q_\perp = C_{in}^E Q_{sep}/(S_p/2)$, where C_{in}^E is the fraction of the heat leaking into the left SOL to the total heat from the core. This study assumes $C_{in}^E = 0.33$ [14]. The symbol S_p is the plasma surface area defined by $S_p = 2\pi R_p 2\pi a_p \sqrt{\kappa}$, where a_p is the minor radius and κ is for the elongation. The fraction f_{imp} is the ratio of impurity radiation losses to the total heat flowing into the left SOL in Fig. 1 (b). The faction f_{imp} is modelled in Sec. 2.3. Symbols $\varepsilon = 21.8\,\mathrm{eV}$ [11] and $\gamma = 7.0$ [15] are the ionization energy of a neutral and the sheath energy transmission coefficient, respectively.

(Local Energy Balance)

The local energy balance is obtained by integrating $\nabla q = Q$, where q and Q are the heat flux and the energy source term, respectively.

$$q_\perp \left(1 - f_{imp}\right) L_s^2 = \frac{4\kappa_0 \Delta_T}{49} \left(T_s^{\frac{7}{2}} - T_d^{\frac{7}{2}}\right). \quad (4)$$

The symbol Δ_T is the decay length of exponential distribution of the temperature in the radial direction. A constant portion of the parallel heat conductivity is given as $\kappa_0 = 1.26 \times 10^3\ (\mathrm{eV})^{-7/2}\,\mathrm{W/m}$.

(Perpendicular Heat Flux)

The perpendicular heat flux is given by $q_{\perp(x)} = -n_s \chi_\perp (\partial T_{s(x)}/\partial x) - 3 T_s D_\perp (\partial n_{s(x)}/\partial x)$ [12], where $\chi_\perp$ and $D_\perp$ are the heat diffusivity and the particle diffusivity, respectively. An exponential distribution in the radial direction is assumed as $n_{s(x)} = n_s \mathrm{e}^{-x/\Delta_n}$ and $T_{s(x)} = T_s \mathrm{e}^{-x/\Delta_T}$. Then we obtain the heat flux on the separatrix surface $q_{\perp(0)} = q_\perp$,

$$q_\perp = \left(\frac{\chi_\perp}{\Delta_T} + \frac{3 D_\perp}{\Delta_n}\right) n_s T_s. \quad (5)$$

2.3 Auxiliary equations

This sub-section provides our assumptions for fractions of ionizations f_{ion}, momentum losses f_{mom}, and radiation losses f_{imp}.

(Ionization faction of neutrals, f_{ion})

The ionization fraction of neutrals emitted from the divertor target, f_{ion}, is calculated as

$$f_{ion} = f_{ion}^{Div} + f_{ion}^{SOL}\left(1 - f_{ion}^{Div}\right), \quad (6)$$

where each of f_{ion}^{Div} and f_{ion}^{SOL} is the ionization fraction of neutrals in the divertor region and the SOL region, respectively. This paper focuses only on hydrogen atoms for neutral particles.

The fraction in the divertor region was modelled as

$$f_{ion}^{Div} = 1 - \exp\left(-\frac{L_d \sin\psi}{\lambda_{ion}^{Div}}\right), \quad (7)$$

where $\lambda_{ion}^{Div} = v_n/n_d\langle\sigma v\rangle_i$ is the ionization mean free path of neutrals. The neutral velocity v_n is calculated by $v_n = \sqrt{T_n/m_i}$ with the neutral temperature T_n. In this paper, T_n is assumed to be 3.0 eV. The ionization reaction rate coefficient of neutrals [16], $\langle\sigma v\rangle_i$, has a strong dependency on the divertor temperature, especially $T_d < 10\,\mathrm{eV}$. It is noted that $L_d \sin\psi$ is the divertor length on the poloidal cross section. The length has been employed as an effective distance for neutrals being ionized in the divertor region. It is because neutrals are free from the magnetic field and assumed to directly approach the SOL on the poloidal cross section.

The fraction in the SOL region was modelled as

$$f_{ion}^{SOL} = \frac{A_{SOL}}{A_{CORE} + A_{SOL} + A_{pump}}, \quad (8)$$

where each of A_{CORE} and A_{SOL} is an effective area for the core region and the SOL region, respectively. In this paper, these effective areas of A_{CORE} and A_{SOL} are assumed to be their cross-sectional area on the plasma midplane, $A_{CORE} = 2\pi R_p a_p$ and $A_{SOL} = 2\pi R_p \Delta_n$. The pumping effect is introduced by the factor of A_{pump}. In the present study, $A_{pump} = 0$ is assumed.

(The fraction of momentum losses, f_{mom})

Neutrals continue to collide with ions and take their momentum through collisions until those neutrals are ionized. As opposite reaction, ions lose their momentum at collisions. The fraction f_{mom} is modelled as an exponential function, a characteristic length of which is assumed to be the charge-exchange mean free path between neutrals and plasma ions, λ_{CX}. The ionization mean free path of neutrals, λ_{ion}, is taken as an effective distance for neutrals continuing momentum losses.

$$f_{mom} = 1 - \exp\left(-\frac{\lambda_{ion}}{C_{mom}\lambda_{CX}}\right), \tag{9}$$

where $\lambda_{CX} = v_n/n_d\langle\sigma v\rangle_{CX}$. The charge-exchange reaction rate coefficient of neutrals [16], $\langle\sigma v\rangle_{CX}$, has a weaker dependency on the divertor temperature compared to $\langle\sigma v\rangle_i$. In this paper, a parameter $C_{mom} = 100$ is introduced so that f_{mom} takes effect when the divertor temperature becomes less than 5 eV.

(The fraction of impurity radiation losses, f_{imp})

The fraction of impurity radiation losses to the total heat flowing into the left SOL from the core in Fig. 1 (b) is assumed as

$$f_{imp} = \frac{2\pi R_p \Delta_E L_d \sin\psi f_c n_d^2 L(T_d)}{q_\perp \frac{S_p}{2}}. \tag{10}$$

Radiation losses are calculated as $P_{rad} = \int_{div} n_{imp} n_d L(T_d) dV$, where n_{imp} is the impurity density and $L(T_d)$ is a cooling rate. The CSD model has employed $L(T_d)$, corresponding to impurity species, as a function of the divertor temperature. On the other hand, [11] assumes a constant value, $L(T_d) = 1.0 \times 10^{-31}\,\mathrm{Wm^3/s}$. This paper evaluated $n_{imp} = f_c n_d$. The value of f_c depends on impurity species. The CSD model has taken a constant f_c described later in the present study, while [11] uses f_c as a parameter.

3. Particle and Energy Balance

3.1 Transformation of basic equations

Five basic Eqs. (1) through (5) have seven unknown variables, $n_s, T_s, n_d, T_d, \Delta_n, \Delta_T$ and Δ_E. The relations among three decay lengths are assumed as described in Sec. 2.1, which reduces the number of variables to five. Now five basic equations can be solved.

In order to solve five basic Eqs. (1) through (5), they were merged into two Eqs. (1) and (3). In the process of this transformation, three unknowns (n_s, T_s and Δ_T) were eliminated. In other words, we obtained the particle balance Eq. (1) and the energy balance Eq. (3) as a function of n_d and T_d. This calculation process is explained as follows.

Substituting Eq. (2) into Eq. (5) with $\Delta_n = (1/2)\Delta_T$ gives

$$\Delta_T(n_d, T_d) = \frac{\chi_\perp + 6D_\perp}{q_\perp} \cdot \frac{\left(1 + M_d^2\right) n_d T_d}{(1 - f_{mom})}. \tag{11}$$

With the use of Eq. (11) and $\Delta_E = (2/7)\Delta_T$, Eq. (10) becomes

$$f_{imp}(n_d, T_d) = \frac{2\pi R_p L_d \sin\psi f_c n_d^2 L(T_d)}{q_\perp \frac{S_p}{2}} \times \frac{2}{7} \cdot \frac{\chi_\perp + 6D_\perp}{q_\perp} \cdot \frac{(1 + M_d^2) n_d T_d}{(1 - f_{mom})}. \tag{12}$$

Variables $\Delta_n, \Delta_T, \Delta_E$ and f_{imp} have been expressed as functions of n_d and T_d so far. Fractions f_{ion} and f_{mom} are originally functions of n_d and/or T_d. Substitution of $\Delta_n, \Delta_T, \Delta_E, f_{imp}, f_{ion}$ and f_{mom} into Eqs. (1) and (3) deletes all the variables but n_d and T_d.

3.2 Particle balance

Equation (1) now has two variables (n_d and T_d) and a parameter Φ_{sep}. In our calculation process, Φ_{sep} was

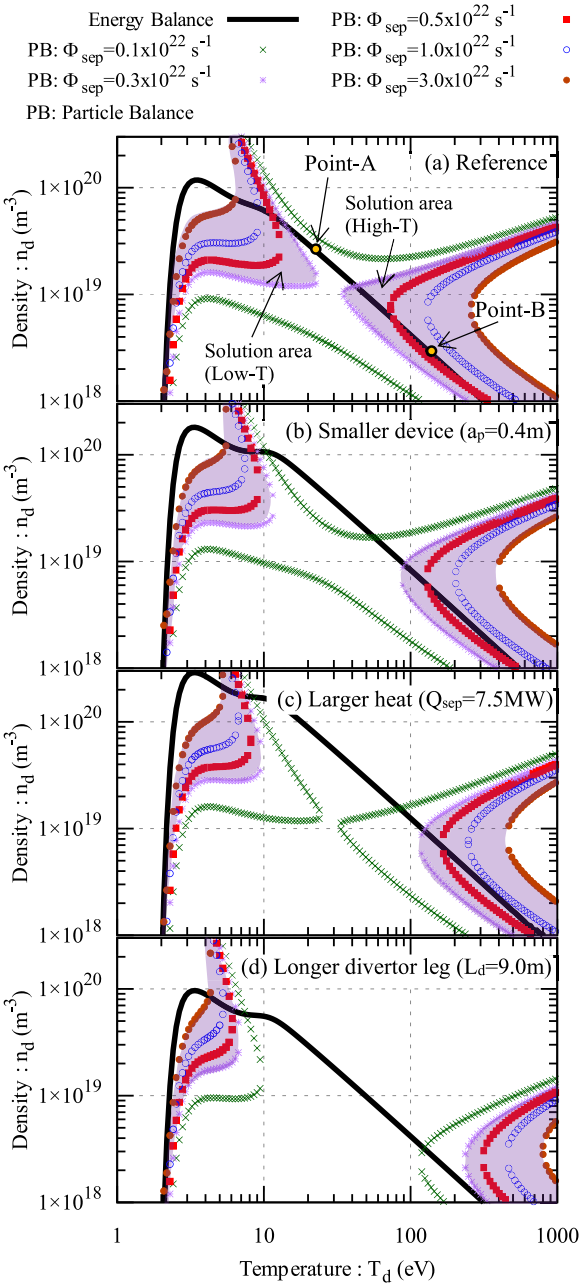

Fig. 2 Particle/energy balances for (a) JT-60U parameters in Table 1 (Reference Case), (b) $a_p = 0.4$ m, (c) $Q_{sep} = 7.5$ MW and (d) $L_d = 9.0$ m. For case (b) through (d), parameters other than those stated above are the same as Reference Case (a). The hatched areas indicate Reference Range of Φ_{sep}. The left hatched area in each graph is for low temperature solutions, while right for high temperature solutions. Case (a) through (c) have high temperature solutions, while (d) has lost them in Reference Range of Φ_{sep}.

fixed. Then, for given T_d, the divertor density n_d satisfying Eq. (1) was solved by a binary method. This process was repeated for five Φ_{sep} values shown in Fig. 2.

3.3 Energy balance

For the energy balance, substituting Eqs. (11) and (12) into Eq. (3) with an assumption of $\Delta_E = (2/7)\Delta_T$ yields

$$-\alpha_E n_d^3 - \beta_E n_d^2 + L_s q_\perp = 0, \tag{13}$$

where

$$\begin{aligned} \alpha_E(T_d) &= \widetilde{f_{imp}}\widetilde{\Delta_E} L_s q_\perp, \\ \beta_E(T_d) &= M_d C_s \widetilde{\Delta_E}(\varepsilon + \gamma T_d), \end{aligned} \tag{14}$$

and

$$\begin{aligned} \widetilde{f_{imp}} &= \frac{2\pi R_p L_d \sin\psi f_c L(T_d)}{q_\perp \dfrac{S_p}{2}} \\ &= f_{imp}/(\Delta_E n_d^2), \\ \widetilde{\Delta_E} &= \frac{2}{7}\frac{(\chi_\perp + 6D_\perp)}{q_\perp}\frac{(1+M_d^2)T_d}{1-f_{mom}} \\ &= \Delta_E/n_d. \end{aligned}$$

A cubic Eq. (13) always has a unique real solution with a positive sign ($n_d > 0$), while the remaining two solutions are real ones with a negative sign ($n_d < 0$) or imaginary ones. Here, only the unique real solution with a positive sign ($n_d > 0$) has a physical meaning. For given T_d, coefficients $\alpha_E(T_d)$ and $\beta_E(T_d)$ are calculated, then n_d is obtained from Eq. (13).

4. Divertor Plasma Characteristics on Temperature-Density Plane under JT-60U Parameters

The particle/energy balances are thoroughly analyzed by using the CSD model with JT-60U parameters [17, 18]. The investigation reveals dependencies of particle/energy balances on key physics and engineering parameters of the device. In addition, Sec. 4.2 discusses requirements for the divertor plasma to have low temperature solutions.

JT-60U parameters used in a simulation are shown in Table 1. The table also has JA-DEMO parameters [7, 8] calculated in Sec. 5. A simulation for a JT-60U case incorporates carbon sputtered on the walls as impurity particles. This paper assumes $f_c = 1.5\times10^{-2}$ [19] as a ratio of n_{imp} to n_d and has employed a cooling rate fitted in Ref. [20] as a function of the divertor temperature. The cooling rate has a local peak of $L(T_d)\sim1.0\times10^{-31}$ Wm^3/s at $T_d\sim7$ eV. On the other hand, for $T_d > 20$ eV, the rate drops by two orders of magnitude.

4.1 Divertor plasma characteristics under JT-60U parameters

Each of the particle and energy balance was independently calculated in a manner described in Sec. 3.2 and Sec. 3.3, respectively. Figure 2 is plotted with "given temperature T_d" as the horizontal axis and "calculated divertor density n_d" as the vertical axis. Particle/energy balance curves are drawn in a wider range than that of realistic physical solutions so that mathematical tendencies can be discussed. Although Fig. 2 has four graphs ((a) - (d)), this sub-section discusses only Fig. 2 (a) which has been calculated with JT-60U parameters shown in Table 1. Figure 2 (a) is "Reference Case" for other calculations in the following sections.

Table 1 Parameter differences: JT-60U vs JA DEMO.

Parameter, (unit)		JT-60U	JA DEMO
Major Radius, (m)	R_p	3.4	8.5
Minor Radius, (m)	a_p	0.8	2.42
Divertor Length (on the magnetic field), (m)	L_d	3.0	32.0
Heat from the core, (MW)	Q_{sep}	2.5	258
Safe factor	q_{eff}	4.7	4.1
Ellipticity	κ	1.5	1.75
Diffusivity (Particle), (m^{2}s^{-1})	$D_\perp$	0.3	0.3
Diffusivity (Heat), (m^{2}s^{-1})	$\chi_\perp$	2.0	1.0

4.1.1 Divertor plasma characteristics

The particle balance strongly depends on Φ_{sep}, which has been used as a parameter in this paper. Figure 2 (a) depicts particle balance curves for five cases of Φ_{sep}. For smaller Φ_{sep} (e.g., $\Phi_{sep} = 1.0\times10^{21}$ s^{-1}), the particle balance has two solutions of n_d in the entire region of temperature as described in Sec. 4.2.2. Hence, it forms two curves for higher n_d and lower n_d as shown in Fig. 2 (a). Both particle balance curves for smaller Φ_{sep} have no intersection with the energy balance curve.

As Φ_{sep} increases, they approach each other in the central area of the figure. The upper one of two particle balance curves makes contact with the energy balance curve at Point-A, $(T_d, n_d)\sim(22, 2.6\times10^{19})$, in Fig. 2 (a). The value of Φ_{sep} giving Point-A is $\Phi_{sep}\sim2.0\times10^{21}$ s^{-1}.

For further increasing Φ_{sep}, two particle balance curves make contact with each other. And then, they again split into left (low temperature region) and right (high temperature region). Therefore, the particle balance loses solutions of n_d in the mid-temperature region. The larger Φ_{sep} becomes, the lower or higher the particle balance curves move in the low or high temperature region, respectively.

Particle balance curves in the high temperature region keep intersections with the energy balance curve until a particle balance curve reaches to go through Point-B, $(T_d, n_d)\sim(135, 2.8\times10^{18})$, in Fig. 2 (a). The value of Φ_{sep} giving Point-B is $\Phi_{sep}\sim5.9\times10^{21}$ s^{-1}. On the other hand, particle balance curves in the low temperature region keep

intersections with the energy balance curve for larger Φ_{sep} values.

The value range of Φ_{sep} for JT-60U is roughly assumed to be around Φ_{sep}~$1.0 \times 10^{22}\,s^{-1}$. Two regions partitioned by particle balance curves for $3.0 \times 10^{21}\,s^{-1} \leq \Phi_{sep} \leq 3.0 \times 10^{22}\,s^{-1}$, hereinafter referred to as "Reference Range of Φ_{sep}", are hatched in Fig. 2. The left partitioned area is for low temperature (Low-T) solutions, while right for high temperature (High-T) solutions.

The energy balance yields only one solution for given T_d as discussed in Sec. 3.3. Therefore, it forms a unique curve. The energy balance curve goes through both Low-T and High-T solution areas established by particle balance curves. Solutions to satisfy both the particle balance and the energy balance are given by intersections of these two curves.

For lower Φ_{sep}, but which is limited in Reference Range of Φ_{sep}, the divertor has both Low-T and High-T solutions. Low-T solutions are obtained in accordance with large f_{ion} (shown in Fig. 3) corresponding to high recycling. On the other hand, High-T solutions come with small f_{ion}, which is interpreted to low recycling. So far, a hysteresis feature has been pointed out for divertor plasmas [21]. Whether Low-T or High-T solution is taken depends on the immediately preceding status of the divertor plasma.

As Φ_{sep} becomes larger, particle balance curves in the high temperature region leave the energy balance curve, while those in the low temperature region keep intersections with the energy balance curve. Therefore, the divertor takes Low-T solutions with high recycling for larger Φ_{sep}. This is a well-known high recycling scenario [11].

4.1.2 Limit of analysis in the current CSD model

The current CSD model has a limit of analysis for low temperature. As the temperature of divertor plasma goes lower, f_{mom} converges to 1.0 in Eq. (9). This (f_{mom}~1.0) takes Δ_n, Δ_T and Δ_E to positive infinity in Eq. (11). The divergence of the decay length is not realistic. The rapid decrease of the energy balance on the left side of its peak is caused by the divergence. Solutions around T_d~2 eV must not be employed as a divertor status.

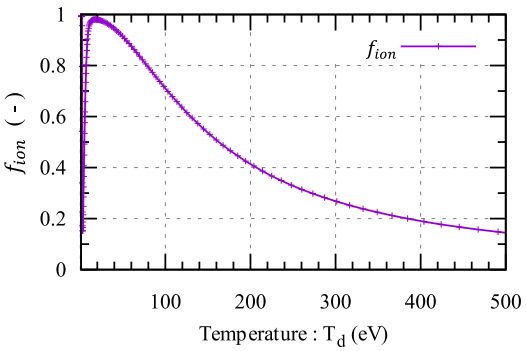

Fig. 3 Ionization faction of neutrals, f_{ion}. A sharp drop within the temperature of M-Segment (20 eV < T_d < 150 eV) causes instability of the particle balance.

The solution trajectory satisfying both the particle and energy balances completely follows the energy balance curve with arbitrary Φ_{sep}. Now, define three temperature segments divided by Point-A and B in Fig. 2 (a); T_d < 22 eV (L-Segment), 22 eV < T_d < 135 eV (M-Segment) and 135 eV < T_d (H-Segment) on the solution trajectory (= the energy balance curve). On L-Segment and H-Segment, n_d rises as Φ_{sep} increases. On the other side, n_d drops as Φ_{sep} increases on M-Segment. The divertor density n_d intuitively seems to become larger as the number of particles coming into SOL Φ_{sep} increases. The opposite characteristic from our insight on M-Segment results from a sharp drop of f_{ion} as n_d decreases. This is explained as follows.

Substituting $C_n = 1.0$ and $N_{puff} = 0$ into Eq. (1) gives

$$C_{in}^N \Phi_{sep} - (1 - f_{ion})\, n_d M_d C_s 2\pi R_p \Delta_n \sin\psi = 0. \quad (15)$$

LHS is originally equivalent to the time differentiation of the total number of particles in SOL and divertor regions in a particle transport equation. LHS is assumed to equal 0 in this research because this study focuses on equilibrium statuses.

Consider a small change in LHS which is induced by a perturbation in an equilibrium solution (T_{d0}, n_{d0}). Assume that the divertor density takes a "negative" perturbation from n_{d0} (T_{d0} generally takes a "positive" perturbation at the same time). This perturbation rapidly makes f_{ion} smaller on M-Segment as shown in Fig. 3. Then, the second term of LHS becomes larger because it is proportional to $(1 - f_{ion})/\sqrt{T_d}$ under an assumption of constant pressure, $n_d T_d$. The first term Φ_{sep} rises with decrease of n_d to keep the particle balance. This means that LHS of Eq. (15) becomes negative when n_{d0} takes a negative perturbation for a fixed Φ_{sep}.

Remember that LHS originally is the time differentiation of the number of particles which is roughly proportional to $\partial n_d/\partial t$. A condition where $\partial n_d/\partial t < 0$ as n_d drops causes a further drop in n_d. It is a typical unstable system. This is what occurs on M-Segment (unstable). Therefore, H-Segment is in the focus for High-T solutions.

4.2 Particle/energy balance analyses to eliminate high temperature solutions

For fusion reactors, Low-T solutions are required as the divertor plasma status. As shown in Fig. 2 (a), however, Reference Case has both Low-T and High-T solutions. In order to keep the divertor plasma at a low temperature, it is required to eliminate High-T solutions. Solutions are obtained by intersections of the particle and energy balance curves. This sub-section provides careful analyses of the particle/energy balance equations to eradicate intersections in the high temperature region. These studies clarify

key physics and engineering parameters to affect relative positions of the particle/energy balance curves. Then, two balance curves are re-drawn with changed parameters and relative positions are investigated whether or not they lose intersections (High-T solutions).

4.2.1 Analysis of the energy balance

The fraction f_{imp} dramatically drops as T_d rises more than 20 eV because of a dependency of carbon cooling rate $L(T_d)$ on the divertor temperature. Therefore, in this temperature range, f_{imp} can be neglected. Then Eq. (13) is easily solved,

$$n_d = \sqrt{\frac{L_s q_\perp}{\beta_E}} \propto \frac{Q_{sep}\sqrt{q_{eff}}}{a_p\sqrt{\kappa R_p(\chi_\perp + 6D_\perp)}}. \tag{16}$$

Equation (16) indicates;

(b) For a smaller device (smaller a_p, R_p), n_d in Eq. (16) becomes larger, which causes the energy balance curve in Fig. 2 (a) to move upper. For a qualitative discussion purpose, an energy balance curve with halved a_p is shown in Fig. 2 (b).
(c) For larger power flowing into the SOL (larger Q_{sep}), n_d in Eq. (16) becomes larger, which causes the energy balance curve in Fig. 2 (a) to move upper. For a qualitative discussion purpose, an energy balance curve with tripled Q_{sep} is shown in Fig. 2 (c).
(d) The divertor length, L_d, does not affect either n_d in Eq. (16) or the energy balance curve. For a qualitative discussion purpose, an energy balance curve with tripled L_d is shown in Fig. 2 (d).

*Bullet characters correspond to sub-characters in Fig. 2.

4.2.2 Analysis of the particle balance

The characteristics of the particle balance are discussed below. Let P be defined as

$$\begin{aligned} P \equiv\ & C_{in}^N \Phi_{sep} - n_d M_d C_s 2\pi R_p \Delta_n \sin\psi \\ & + f_{ion}\left(C_n n_d M_d C_s 2\pi R_p \Delta_n \sin\psi + N_{puff}\right). \end{aligned} \tag{17}$$

Here, $P = 0$ is the particle balance Eq. (1). As described in Sec. 2.2, the present study assumes $N_{puff} = 0$ and $C_n = 1.0$. In Eq. (8), $A_{CORE} \gg A_{SOL}$ leads f_{ion}^{SOL}~0. Thus, f_{ion} can be approximated as follows,

$$\begin{aligned} f_{ion} &= \left\{f_{ion}^{Div} + f_{ion}^{SOL}\left(1 - f_{ion}^{Div}\right)\right\} \\ &\approx f_{ion}^{Div} \\ &= 1 - \exp\left(-\frac{L_d \sin\psi}{\lambda_{ion}^{Div}}\right). \end{aligned} \tag{18}$$

Substituting these into Eq. (17) gives

$$\begin{aligned} P = & C_{in}^N \Phi_{sep} - n_d M_d C_s 2\pi R_p \Delta_n \sin\psi \\ & \times \exp\left(-\frac{L_d \sin\psi}{\lambda_{ion}^{Div}}\right). \end{aligned} \tag{19}$$

With the use of

$$\begin{aligned} \Delta_n &= \frac{1}{2}\frac{(\chi_\perp + 6D_\perp)}{q_\perp}\frac{(1+M_d^2)n_d T_d}{1 - f_{mom}} \\ &= \widetilde{\Delta_n} n_{d,} \end{aligned}$$

where

$$\widetilde{\Delta_n} = \frac{1}{2}\frac{(\chi_\perp + 6D_\perp)}{q_\perp}\frac{(1+M_d^2)T_d}{1 - f_{mom}},$$

we obtain

$$\begin{aligned} P &= C_{in}^N \Phi_{sep} - n_d M_d C_s 2\pi R_p \widetilde{\Delta_n} n_d \sin\psi \\ &\quad \times \exp\left(-L_d \sin\psi \frac{n_d \langle\sigma v\rangle_i}{v_n}\right) \\ &= C_{in}^N \Phi_{sep} - \beta_P n_d^2 \exp(-\alpha_P n_d), \end{aligned} \tag{20}$$

where

$$\begin{aligned} \alpha_P(T_d) &= L_d \sin\psi \frac{\langle\sigma v\rangle_i}{v_n}, \\ \beta_P(T_d) &= M_d C_s 2\pi R_p \widetilde{\Delta_n} \sin\psi. \end{aligned} \tag{21}$$

A function $P(n_d)$ has a minimum value at $n_d = 2/\alpha_P$ for $n_d > 0$ and $P(0) = P(\infty) = C_{in}^N \Phi_{sep}$. Therefore, the necessary and sufficient condition for Eq. (20) to have solution(s) is

$$P(2/\alpha_P) = C_{in}^N \Phi_{sep} - \frac{4\beta_P}{\alpha_P^2} e^{-2} \le 0. \tag{22}$$

When Φ_{sep} and T_d are given, $P(n_d)$ has a unique solution for $P(2/\alpha_P) = 0$ or two solutions for $P(2/\alpha_P) < 0$.

Inequality (22) determines an allowable maximum value of Φ_{sep}, hereinafter referred to as $\Phi_{max}(T_d) = (4\beta_P/C_{in}^N\alpha_P^2)e^{-2}$. Figure 4 shows a curve of $\Phi_{max}(T_d)$ with

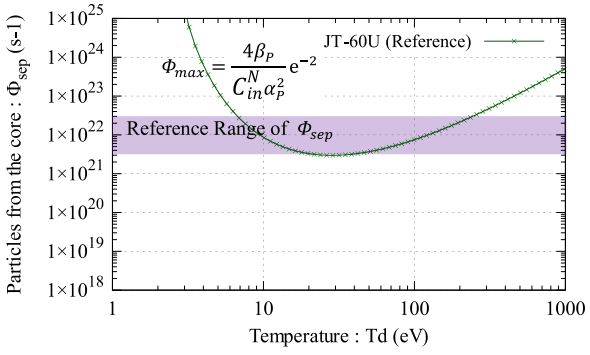

Fig. 4 The necessary and sufficient condition for the particle balance to have solution(s); $\Phi_{sep} \le \Phi_{max}(T_d) = (4\beta_P/C_{in}^N\alpha_P^2)e^{-2}$. The hatched area shows Reference Range of Φ_{sep}. This graph indicates the particle balance Eq. (1) is likely to lose solutions in the mid- temperature region. When the curve moves downward, the particle balance curves in Fig. 2 (a) change the position to far lower/higher in the low/high temperature region, respectively.

Reference Range of Φ_{sep}. When Φ_{sep} is given, a particle balance for the Φ_{sep} value has solutions in the T_d range where $\Phi_{sep} \leq \Phi_{max}(T_d)$ holds. As an example, $\Phi_{max}(T_d)$ goes under $\Phi_{sep} = 1.0 \times 10^{22}\,\mathrm{s}^{-1}$ around 10 eV $< T_d <$ 120 eV in Fig. 4. Therefore, the particle balance for $\Phi_{sep} = 1.0 \times 10^{22}\,\mathrm{s}^{-1}$ in Fig. 2 (a) has no solution in the T_d range. This is the reason why particle balance curves bifurcate into low temperature or high temperature region. The larger Φ_{sep} becomes, the lower or higher the particle balance curves move in the low or high temperature region, respectively.

Figure 2 (a) indicates that particle balance curves possibly lose intersections with the energy balance curve in the high temperature region if they move rightward, much higher temperature position. In order to move them rightward, it is effective to push the curve of $\Phi_{max}(T_d)$ down in Fig. 4. It is equivalent to making $\Phi_{max}(T_d)$ smaller.

The value of $\Phi_{max}(T_d)$ is proportional to some physics and engineering parameters as shown in Eq. (23).

$$\Phi_{max} = \frac{4\beta_P}{C_{in}^N \alpha_P^2} \mathrm{e}^{-2} \propto \frac{R_p^2 a_p (\chi_\perp + 6D_\perp)\sqrt{\kappa}}{Q_{sep} L_d^2 \sin\psi}. \quad (23)$$

Parameters with a large margin of adjustment are a_p, R_p, Q_{sep}, L_d. Equation (23) indicates that the particle balance curves in the high temperature region in Fig. 2 (a) move rightward, when

(b) the size of a device is reduced (reduction of a_p and/or R_p),
(c) the heat flowing into the SOL becomes higher (increase in Q_{sep}) or
(d) the divertor length becomes longer (extension of L_d).

*Bullet characters correspond to sub-characters in Fig. 2. Re-calculated particle balance curves are shown in Figs. 2 (b) through (d), respectively.

4.2.3 Parameter surveys

This sub-section discusses relative positions between shifted particle/energy balance curves whether or not they lose intersections in the high temperature region. As described in Sec. 4.2.2, (b) reduction of a_p and/or R_p, (c) increase in Q_{sep} and/or (d) extension of L_d possibly let particle balance curves leave the energy balance curve in the high temperature region. Parameters surveyed in this study are; (b) $a_p = 0.4$ m, (c) $Q_{sep} = 7.5$ MW and (d) $L_d = 9.0$ m. Particle/energy balance curves for these three cases are redrawn in Figs. 2 (b) through (d). It is noted that parameters other than those stated for each case are the same as Reference Case (a).

In case (b), the minor radius a_p was halved. This has an effect to bring particle balance curves to both sides. At the same time, a reduction of the minor radius has changed the position of the energy balance curve to a higher density side (upper side in Fig. 2 (b)) in accordance with Eq. (16). As a result, the divertor plasma keeps High-T solutions, even though particle balance curves have moved to higher temperature position to leave the energy balance curve in Reference Case.

In case (c), the heat crossing over the separatrix Q_{sep} was tripled. Qualitative characteristics are the same as those for case (b).

In case (d), the divertor length L_d was tripled. As Eq. (23) indicates, Φ_{max} decreases by the square of L_d, which pushes particle balance curves to lower/higher temperature sides. On the other side, n_d in Eq. (16) does not depend on L_d. Therefore, the energy balance curve remains at the same place in the high temperature region. This characteristic has an effect to take particle balance curves away from the energy balance curve. As a result, the divertor plasma does not have High-T solutions for $\Phi_{sep} \geq 3.0 \times 10^{21}\,\mathrm{s}^{-1}$ and it stays at low temperature.

For summary, the CSD model shows the following dependencies of the divertor plasma on the key physics and engineering parameters of fusion devices.

1) For lower Φ_{sep} *, the divertor has both Low-T and High-T solutions. (Fig. 2 (a))
2) For higher Φ_{sep} *, the divertor has only Low-T solutions with high recycling. (Fig. 2 (a))
3) For a smaller device*, the divertor temperature of High-T solution becomes higher. (Fig. 2 (b))
4) For larger heat from the core*, the divertor temperature of High-T solution becomes higher. (Fig. 2 (c))
5) For a longer divertor length*, the divertor temperature becomes lower. (Fig. 2 (d))

* Parameters other than those stated are fixed for this study.

5. Divertor Plasma Analyses for JA DEMO

The CSD model was applied to a future demonstration-class size reactor in order to confirm its validity for different sizes of devices. In this paper, JA DEMO reactor was chosen, major physics and engineering parameters of which were shown in Table 1. JA DEMO is currently under study to equip increased divertor volume so as to increase the radiation power and to reduce the divertor plasma temperature [8]. In Refs. [7, 8], it is reported a SONIC result indicates that both ion and electron temperature decrease to around 1 eV when "Detachment" is achieved.

This section reports analyses of JA DEMO divertor plasma with the use of the CSD model. For JA DEMO, tungsten is the main candidate for divertor plates. The erosion of tungsten is not expected to be significant in terms of cooling down the divertor plasma. Rather, injected argon or other noble gas contributes to radiation. Therefore, the CSD model implemented argon for a simulation. Also, carbon which has been employed for a JT-60U simulation is calculated as a reference. Reference

[8] reported that the value of f_c for argon varies around $f_c \sim 1.0 \times 10^{-2}$ with a spatial distribution. This paper assumes $f_c = 1.5 \times 10^{-2}$ for argon to have the same precondition employed for carbon in the JT-60U simulation. The cooling rate for argon is calculated to follow Ref. [22] as a function of the divertor temperature. The rate has a local peak of $L(T_d) \sim 1.0 \times 10^{-31}$ Wm^3/s at $T_d \sim 13$ eV.

5.1 The condition for the particle balance to have solutions

The necessary and sufficient condition for the particle balance of JA DEMO to have solution(s), $\Phi_{sep} \leq \Phi_{max}(T_d) = (4\beta_P / C_{in}^N \alpha_P^2) e^{-2}$, is shown in Fig. 5, which also depicts that of JT-60U Reference Case for a comparison. The curve for JA DEMO is far below that for JT-60U because of a longer divertor length. Now, Φ_{sep} of JA DEMO is roughly assumed to be around $\Phi_{sep} \sim 1.0 \times 10^{22}$ s^{-1} or more. For this range of Φ_{sep}, T_d becomes around 3 eV with a small dependency on Φ_{sep}. Therefore, Fig. 5 indicates that the JA-DEMO divertor has only Low-T solutions ($T_d < 3$ eV) unlike JT-60U Reference Case.

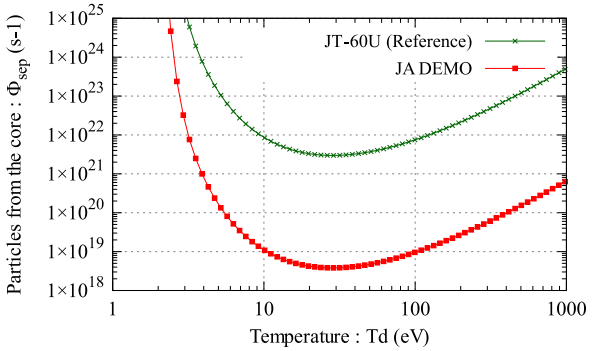

Fig. 5 The necessary and sufficient condition for the particle balance Eq. (1) to have solution(s) for JT-60U and JA DEMO. The curve for JA DEMO is far below that for JT-60U because of a longer divertor length, which prevents JA DEMO from having high temperature solutions.

5.2 Divertor plasma analyses

Each of the particle and energy balance is independently calculated in the same manner as for the JT-60U case (Sec. 4.1). Their balances are drawn on (T_d, n_d) plane in Fig. 6.

The particle balance for $\Phi_{sep} \sim 1.0 \times 10^{22}$ s^{-1} or more, as described in Sec. 5.1, has solutions below $T_d \sim 3$ eV. Unlike JT-60U case (Fig. 2), it does not give any solutions in the high temperature region of the figure.

The energy balances of JA DEMO with carbon or argon as impurity are shown in Fig. 6. The fraction of impurity radiation losses, f_{imp}, has a local peak around a peak of the cooling rate of each impurity species. Around the f_{imp} peak, the first term in RHS of Eq. (3) becomes larger, which makes the other terms relatively smaller. This means a decrease of n_d. The local peak of the cooling rate for carbon/argon is around 7 eV/13 eV, respectively. The energy balances for each impurity species form a local bottom around the local peak of the cooling rate.

The cooling rate of argon is smaller than that of carbon below $T_d \sim 8$ eV. In this temperature range, the total energy of the divertor plasma is larger when argon is injected as impurity. Therefore, the energy balance curve for argon surpasses that for carbon in the temperature range. On the other hand, argon keeps effective around $T_d \sim 20$ eV, which leads the energy balance curve for argon lower than that for carbon.

The CSD model has shown a low temperature state of its divertor plasma as has been already reported by a SONIC simulation. This result has proven the CSD model can cover a wide range of device sizes, which is required for design studies of future fusion reactors.

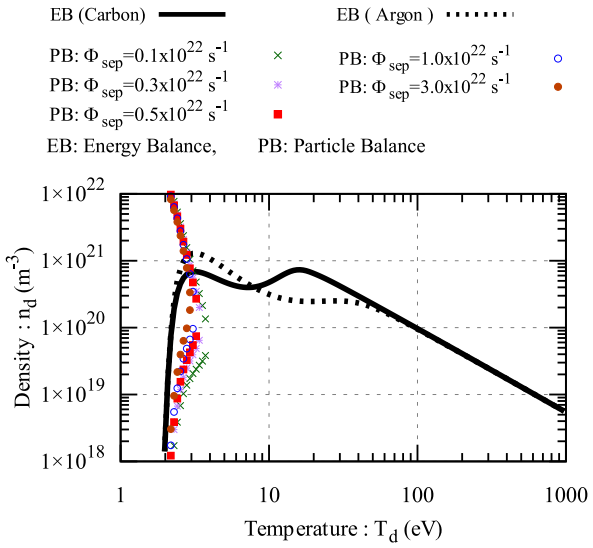

Fig. 6 Particle/energy balance for JA DEMO parameters with carbon/argon as impurities. Around the radiation peak temperature of each impurity, the energy balance has a local bottom. It is noted that the impurity species does not affect the particle balance, though it makes changes in the energy balance.

6. Summary

This paper has analyzed divertor plasma characteristics by using the CSD model with parameters of JT-60U. The discussion evaluated dependencies of particle/energy balances on key physics and engineering parameters of the device. The CSD model has identified three physics and engineering parameters which strongly affect the divertor temperature; (1) divertor length, (2) major/minor radius and (3) heat from the core. It has been shown that a longer divertor leg eliminates high temperature solutions.

Section 5 simulated the divertor plasma for a demonstration-class tokamak (JA DEMO). The extension of the divertor leg length in JA DEMO keeps the particle

balance in low temperature, which holds intersections with the energy balance around the temperature. This low temperature state of the divertor plasma is consistent with a simulation result SONIC has shown.

These results have proven the CSD model can cover a wide range of device sizes. The CSD model is applicable to basic studies of directions and design concepts for fusion reactors.

[1] H. Kawashima *et al*., Plasma Fusion Res. **1**, 31 (2006).
[2] K. Shimizu *et al*., Nucl. Fusion **49**, 065028 (2009).
[3] S. Wiesen *et al*., J. Nucl. Mater. **463**, 480 (2015).
[4] X. Bonnin *et al*., Plasma Fusion Res. **11**, 1403102 (2016).
[5] F. Subba *et al*., Contrib. Plasma Phys. **58**, 758 (2018).
[6] F. Subba *et al*., Nucl. Fusion **61**, 106013 (2021).
[7] N. Asakura *et al*., Nucl. Fusion **61**, 126057 (2021).
[8] N. Asakura *et al*., Processes **10**, 872 (2022).
[9] R. Hiwatari *et al*., Contrib. Plasma Phys. **44**, 76 (2004).
[10] R. Hiwatari *et al*., J. Nucl. Mater. **337-339**, 386 (2005).
[11] R. Hiwatari *et al*., Contrib. Plasma Phys. **48**, 174 (2008).
[12] K. Borrass, Nucl. Fusion **31**, 1035 (1991).
[13] W.D. Langer *et al*., IEEE Trans. Plasma Sci. **PS-13, No.9**, 163 (1985).
[14] A. Hatayama *et al*., J. Nucl. Mater. **290-293**, 407 (2001).
[15] P. Stangeby, The Plasma Boundary of Magnetic Fusion Devices (Institute of Physics Publishing, 2000) P.94.
[16] D. Reiter, The data file HYDHEL: Atomic and Molecular Data for EIRENE based upon: Janev, Langer, Evans, Post, "Elementary Processes in Hydrogen-Helium Plasmas", ver. Jan. 13, 2020.
[17] A. Hatayama *et al*., Nucl. Fusion **40**, 2009 (2000).
[18] N. Asakura *et al*., J. Nucl. Mater. **241-243**, 559 (1997).
[19] N.A. Uckan *et al*., ITER PHYSICS DESIGN GUIDELINES, 1989.
[20] D.E. Post *et al*., Atomic Nucl. Data Tables **20**, 397 (1977).
[21] D.E. Post *et al*., J. Nucl. Mater. **121**, 171 (1984).
[22] OPEN-ADAS, https://open.adas.ac.uk/, accessed on 28 Apr. 2024.